Chelating Phosphine Ligand Stabilized AuNPs in Methane Detection

Cen Tang, Kang Hee Ku, Shao-Xiong Lennon Luo, Alberto Concellón, You-Chi Mason Wu, Ru-Qiang Lu, Timothy M. Swager*

Department of Chemistry, Massachusetts Institute of Technology (MIT), Cambridge, MA 02139, USA

ABSTRACT: The capping reagent plays an essential role in the functional properties of gold nanoparticles (AuNPs). Multiple stimuli responsive materials are generated *via* diverse surface modification. The ability of the organic ligand shell on gold surface to create a porous shell capable of binding small molecules is demonstrated as an approach to detect molecules, such as methane, that would be otherwise difficult to sense. Thiols are the most studied capping ligands of AuNPs used in chemiresistors. Phosphine capping groups are usually seemed as stabilizers in synthesis and catalysis. However, by virtue of the pyramidal shape of triarylphosphines, they are natural candidates to create intrinsic voids within the ligand shell of AuNPs. In this work, surface functionalized (capped) AuNPs with chelating phosphine ligands are synthesized *via* two synthetic routes, enabling chemiresistive methane gas detection at sub-100 ppm levels. These AuNPs are compared to thiol capped AuNPs, and studies were undertaken to evaluate structure-property relationships for their performance in the detection of hydrocarbons. Polymer overcoatings applied to the conductive networks of the functionalized AuNP arrays were shown to reduce resistivity by promoting the formation of conduction pathways with decreased core-core distance between nanoparticles. Observations made in the context of developing methane sensors, provides insight relevant to applications of phosphine or phosphine containing surface groups in functional AuNP materials.

KEYWORDS: *methane detection, gold nanoparticles, functionalization of gold nanoparticles, porous ligand shell, phosphine-containing functional materials*

Colloid gold nanoparticles (AuNPs) are the most widely studied metal NPs with applications in organic photovoltaics, chemical and biological sensing, imaging, drug delivery, photothermal therapy, electronic conductors, and catalysis.[1-4] For decades thiols have been widely used to stabilize AuNPs as a result of their strong binding affinity and availability.[5-7] More recently, N-heterocyclic carbene (NHC) capped AuNPs are emerging as interesting materials as a result of their outstanding stability.[8-10] Phosphine ligands are among the most widely studied ligands in organometallic and coordination chemistry, and were also first shown to stabilize AuNPs approximately 40 years ago[11] with a number of addition studies since.[12-16] However, applications of phosphine capped AuNPs have mainly focused on asymmetric catalysis[17-18] or the creation of precursors for the synthesis of AuNPs capped with other ligands.[19-20] The limited scope of these capping agents in NP device applications are largely the result of their susceptibility to oxidation[21] and the fact that they promote the formation of ultra-small particles during synthesis. The latter feature encountered when synthesizing phosphine stabilized NPs directly restricts AuNP performance in key applications such as the formation of materials capable of displaying chemiresistance or plasmonic properties.

Of interest to the present study is that the general conical shape of triarylphosphine containing NP capping ligands can create voids capable of binding methane. This general attribute has been recognized wherein phosphine-derived functional units have been used to create porous organic polymers.[22-23] Specific to our interest in chemical sensors, we have targeted phosphine ligands bound to AuNP surface to create conductive materials that display changes in resistivity in response to the absorption of gases or molecular vapors.

The detection of methane at trace levels is of great importance to enable technologies for environmental protection through the minimization of this greenhouse gas and for safety as a result of the explosive nature of methane-air mixtures.[24-25] However, methane sensing is extremely challenging as a result of its lack of a dipole, inert character, high volatility, and small size. Although methane can be detected with metal oxide based chemiresistors, these sensors operate at high temperature and display similar responses to other hydrocarbons.[26-27] An alternative approach is to employ selective absorptive coatings and designed host molecules have enabled methane detection using a quartz crystal microbalance (QCM) detection platform.[28] Herein, we report our studies with emphasis on the utility of aromatic phosphine ligand capped AuNPs for chemiresisitve methane detection, along with synthetic approaches as well as a conductivity-tuning strategy for these NPs.

RESULTS AND DISCUSSION

We started our investigations by synthesizing triphenylphosphine (PPh_3, **L1a**) capped AuNPs. We initially employed the typical Brust synthetic method,[13] and as a result of the low stability of the materials, we did not obtain meaningful sensing signals at 1% of methane concentrations. Thus, we utilized a one-phase synthetic strategy in benzene reported by Stucky and coworkers (Scheme 1, *Path A*) to avoid purification processes that would lead to degradation of the phosphine ligand shells.[29] When the reaction temperature is run at 80 °C, we observe full conversion of AuNPs from $AuCl(PPh_3)$ in a relatively short reaction time.

To our delight, these simple **L1a** capped AuNP materials displayed normalized resistance changes ($\Delta G/G_0$) of 0.02 %

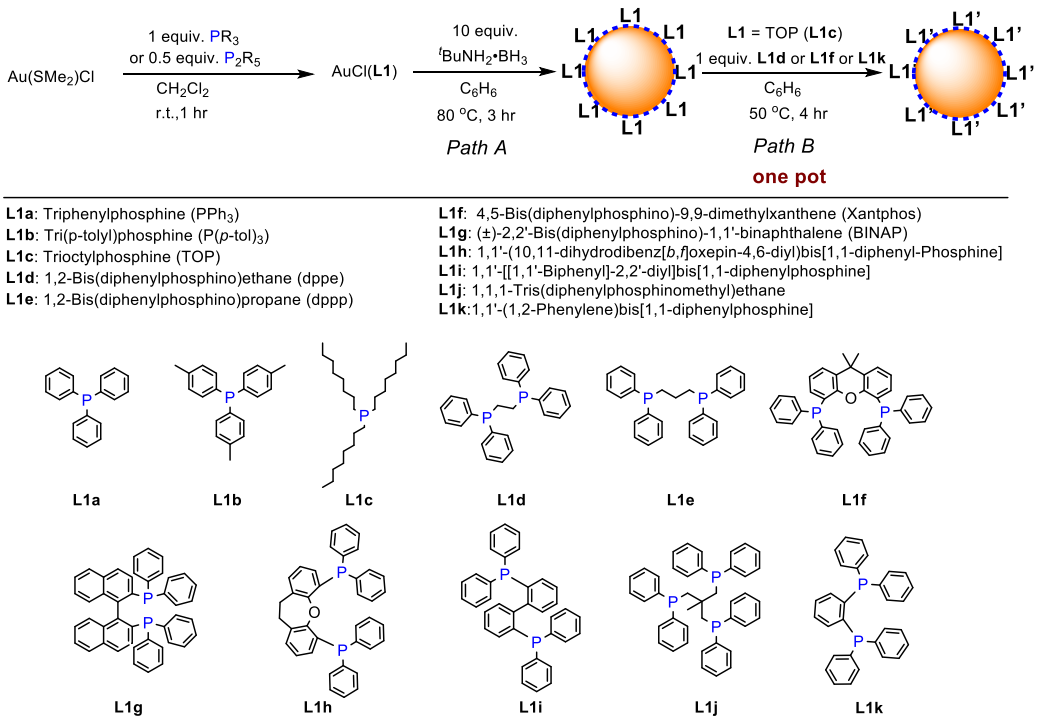

Scheme 1. Synthesis of phosphine ligand (L1) capped AuNPs.

when exposed to 200 ppm methane (Figure 1a, yellow, $\Delta G/G_0$ (%) = $(R_0 - R)/R_0 \times 100$, where R_0 is the initial resistance). These results revealed that phosphine ligand capped AuNPs, may be made to be sufficiently stable for chemiresistive sensing with appropriate synthetic methodologies. With such one-phase synthetic strategy, we later investigated AuNPs capped with the larger-cone-angle tri(*p*-tolyl)phosphine (P(*p*-tol)$_3$, (**L1b**), which exhibited slightly higher sensitivity at 1000 ppm of methane (Table 1) and was able to generate normalized resistance change of 0.02% for 143 ppm methane (Figure 1a, grey). However, both **L1a** and **L1b** suffer from poor oxidative stability, with the PPh_3 bound to the AuNPs decomposing within 48 hrs under ambient conditions. ^{31}P NMR revealed that triphenylphosphine oxide was rapidly formed by oxidation of **L1a** bound to the AuNPs (Figure 1b). This result is also supported by the X-ray photoelectron spectroscopy (XPS) P_{2p} peaks at a binding energy of 134 eV, which are diagnostic of the presence of phosphine oxides and a similar signal was also observed for AuNP capped with **L1b** (Figure 1c). Additionally, we find that, as a result of poor stability, the phosphorus content varies from batch to batch. This oxidative instability leads to a loss of the chemiresistive response to methane (Figure 1d). Freshly prepared **L1a** capped AuNPs give a strong response to 1000 ppm of methane, but after 48 hours they can only respond to 5% (50000 ppm) methane concentrations and after 14 days have no detectable methane response.

To improve stability, we investigated 1,3-bis(diphenylphosphino)propane (dppp, **L1e**) as a chelating capping ligand. **L1e** capped AuNPs can be synthesized from $HAuCl_3 \cdot 3H_2O$ in 2 steps after initial reduction by dimethyl sulfide (SMe_2) to give AuCl(SMe_2). In this process, ligand exchange generates phosphine ligated gold complex AuCl(**L1e**),[30] and reduction of this complex creates the capped nanoparticles (Scheme 1, *Path A*). The **L1e** capped AuNPs from this method display *ca.* 0.1% response to 1000 ppm methane, and maintain this sensitivity after exposure to ambient atmosphere for 2 weeks (Figure 1d). Moreover, it shows a 0.025% response to 100 ppm methane (Figure 1a, blue) and therefore exhibits a clear enhancement of performance over the simpler non-chelating phosphines discussed earlier.

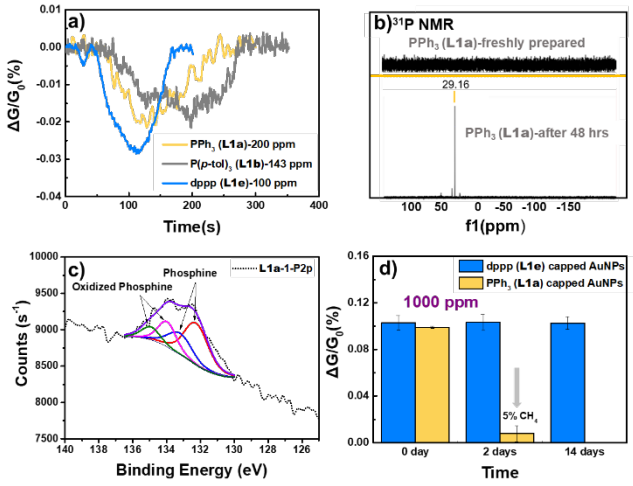

Figure 1. a) Sensing responses of PPh_3 (**L1a**, yellow), P(p-tol)$_3$ (**L1b**, grey), dppp (**L1e**, blue) capped AuNPs at 200 ppm, 143 ppm, 100 ppm of methane. b) ^{31}P NMR of PPh_3 (**L1a**) capped AuNPs. Top: Freshly prepared, where PPh_3 is bound to the AuNP surface and not in solution. Bottom: After 48 hrs, a signal at 29.16 ppm appears, which corresponds to desorbed Ph_3PO. c) P2p XPS spectra of **L1a** capped AuNPs. d) Sensing response changes of PPh_3 (**L1a**) and dppp (**L1e**) capped AuNPs over time. The responses are for 1000 ppm and after 48 hrs the **L1a** device required a 5% concentration of methane to display a response. The error bars are determined from 3 or more devices.

Based on these promising results, we screened a series of commercially available chelating phosphine ligands (**L1d-L1k**, Scheme 1). **L1d-L1j** capped AuNPs are synthesized by the aforementioned procedure. However, this synthetic method does not work in all cases and we observed insoluble black precipitate during the ligand exchange step from $Au(SMe_2)Cl$ to AuCl(**L1k**).

To obtain **L1k** capped AuNPs, and to potentially broaden the scope of phosphine capped AuNPs under mild synthetic and purification conditions, we targeted ligand exchange on preformed nanoparticles. In previous studies of phosphine capped NPs, complete phosphine-phosphine ligand exchange in $CHCl_3$ solutions was observed during the synthesis of palladium NPs.[31] In these Pd NPs, the trioctylphosphine ligand (TOP, **L1c**) was employed as a labile NP stabilizer. Inspired by this work, **L1c** capped AuNPs were synthesized *via Path A*, and **L1k** was then added *in situ* to the crude reaction mixture (Scheme 1**,** *Path B*). XPS analysis reveals that **L1c** is easily oxidized in air within hours, while the bidentate ligands bound to the AuNPs are stable without apparent oxidation after days of exposure to ambient atmosphere (Figure S3). The reaction time for this synthetic process was optimized with the assistance of XPS analysis, which was used as detailed below to monitor the complete exchange (Figure 2a).

We initially ran the exchange reaction with **L1k** for 2 hours at 50 ºC, followed by washed the NPs with toluene and air drying overnight. These samples contained phosphine oxide as indicated by the P_{2p} peaks with binding energy of 134 eV in the XPS spectrum. Given the oxidative sensitivity of TOP (**L1c**), it is assumed that this peak is associated with trioctylphoshine oxide bound to the AuNPs. However, prolonging the phosphine exchange reaction time to 4 hrs, followed by solvent washing and drying, results in purified materials that do not contain phosphine oxides, thereby suggesting that all of **L1c** has been replaced with the more oxidatively stable **L1k**. It is noteworthy that the diameter (*d*) of **L1c** capped AuNPs are initially 3.19 ± 0.99 nm as determined by transmission electron microscopy (TEM) and UV-Vis spectroscopy (Figure 2, green). However, after **L1k** ligand exchange, the nanoparticles have grown to *d* = 4.43 ± 0.87 nm (Figure 2, blue). It appears that the exchange reaction promotes Ostwald ripening. TOP (**L1c**) exchange reactions have seen comparatively little investigation relative to PPh_3 (**L1a**) in phosphine-phosphine exchange reactions on gold clusters.[32] Examples of phosphine capped AuNPs with similarly large sizes (> 3.5 nm) have been reported,[33,34] but the synthesis is generally accomplished with the aid of halide containing surfactants such as tetraoctylammonium bromide to control the NP synthesis, prior to phosphine addition. Ionic surfactants complicate purification and require problematic water and ethanol washes that can compromise the phosphine ligand shell. It is also worth noting that direct NP synthesis in the presence of chelating phosphine ligands promotes the formation of very small NPs that are 1-2 nm in diameter.[12-18] In our prior investigations, it was observed that mono phosphine ligands (**L1a-L1c**) produced AuNPs that are approximately *d* = 3 nm, while bidentate ligands (**L1d-L1j**) lead to smaller gold cores at *ca.*1-2 nm. The exception was BINAP (**L1g**) which gave a *d* = 3.31 ± 0.33 nm (Table 1, Figure S1). These general trends are likely related to tighter binding of most chelating phosphines to the NP surface, which stabilizes the higher energy smaller NPs and limits Ostwald ripening. Surface plasmon resonance effects require larger core sizes,[35] and hence the synthesis of larger gold clusters with a diversified surface functionalization may find applications in Raman spectroscopy.

The purification of AuNPs for sensing experiments is accomplished by dispersing in benzene or toluene (3X) followed by separation by centrifuging at 10000 rpm for 10 min. In this method, material that is not directly attached to the NPs is extracted into the solvent, and generates phosphine oxide-free homogenous materials with 25-33% P(III) content as determined by XPS (Table S1, Figure S3). All observations are consistent with the formation of intact phosphine ligand shell on gold surface of the purified NPs. Chemiresistive sensors are fabricated by drop-casting purified AuNPs (20 mg/mL, 8 µL) from a suspension of toluene onto interdigitated platinum electrodes (5 µm inter-electrode spacing). Sensing experiments to make comparisons across all of the materials investigated were conducted using N_2 as an inert carrier gas, and the current is recorded with a 0.1 V bias applied across the electrodes. Minor linear baseline corrections are applied to account for signal drift. Table 1 summarizes the diameters, base resistances and $\Delta G/G_0$ responses of phosphine capped AuNPs to 1000 ppm methane. Chelating ligands capped AuNPs show higher resistances that can be attributed to the reduced NP size. Smaller particles are less able to stabilize charge separation that is required for electrical conduction and Neugebauer and Webb's model shows an exponential correlation between changes in diameter and activation energy for electron hoping in small NPs.[36] In the case of BINAP (**L1g**) that produced larger AuNPs, the high resistance can be attributed to a larger core-core separation resulting from the larger space occupied by the naphthyl groups. Indeed, interparticle electron tunneling probability decreases exponentially with increasing width of tunneling barriers. As revealed in Table 1, the majority of the phosphine AuNP materials examined showed chemiresistive responses to methane, and those that didn't respond (dppe (**L1d**), **L1i**, **L1j**) displayed much higher base resistances.

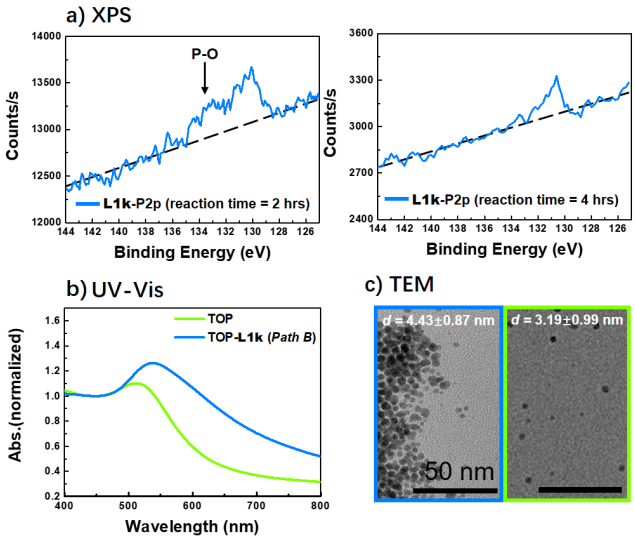

Figure 2. a) P2p XPS spectra of **L1k** capped AuNPs synthesized in 2 hrs and 4 hrs *via Path B*. b) UV-Vis spectra of TOP (**L1c**, green) and **L1k** (blue) capped AuNPs. c) TEM images of TOP (**L1c**, green), and **L1k** (blue) capped AuNPs.

In an effort to create more robust devices, we have experimented with the application of a porous polymer overcoating on fabricated phosphine AuNP devices. In particular, we have used a OMe-ROMP polymer (Brunauer–

Emmett–Teller (BET) surface area = 146 m^2g^{-1}) developed in our laboratory (Figure 3a) that has a flexible backbone, but generates porosity through rigid extended sidechains.[37] Our hypothesis was that non-compliant nature of the sidechains can provide rigidity and can also be used to create a barrier coating to prevent fouling of the sensor and ideally minimize humidity interference. To investigate these effects, we overcoated Xantphos (**L1f**) capped AuNPs devices. After drop-casting OMe-ROMP (30 µL, 2mg/mL, CH_2Cl_2) onto the surface of **L1f** capped AuNPs, the resistance is significantly reduced from 6 MΩ to 0.8 MΩ. This result, suggests that the polymer results in some reorganization of the NP network. This is confirmed by small-angle X-ray scattering (SAXS) studies which reveal that the range of core-core distances reduce slightly from 2.66 nm to 2.58 nm (Figure 3b). As would be expected, the entire diffraction intensity doesn't shift to higher q, but broadens. These observations indicate that the resistance change is likely the result from shortened core-core distance between the particles proximate to the polymer while other AuNPs are not affected. Most importantly, the polymer overlayer doesn't compromise the methane sensing performance of the **L1f** capped AuNPs (Figure 3c), and the response at 500 ppm methane is essentially unchanged by this treatment.

L1	Diameter (nm)[a]	Resistance (Ω)	ΔG/G₀ (%) at 1000 ppm
L1a	3.12 ± 0.68	600	0.10
L1b	3.68 ± 0.83	600	0.11
L1d	1.21 ± 0.27	>200M	/
L1e	1.73 ± 0.39	1M	0.10
L1f	1.84 ± 0.42	6M	0.20
L1g	3.31 ± 0.33	10M	0.08
L1h	1.92 ± 0.28	2M	0.12
L1i	1.93 ± 0.46	>200M	/
L1j	1.65 ± 0.24	~200M	/
L1k	4.43 ± 0.87	6M	0.10

[a] Determined by TEM.

Table 1. Diameters, resistances and sensing responses of phosphine capped AuNPs at 1000 ppm of methane.

To further explore the utility of the polymer overlayer, and to make comparisons with better known thiol based coatings used in AuNP based chemiresistors, we prepared AuNP sensors capped with 1-decanethiol (**L2a**) and 1,9-nonanedithiol (**L2b**)/1-decanethiol(**L2a**) (1/50 mole ratio) (Figure 3d; details in the SI). Alkanethiol capped AuNPs have been studied for hydrocarbon detection including hexane,[38] and the 1/50 composition with the minority component of 1,9-nonanedithiol(**L2b**) has been used to decrease thermal motion and reduce resistivity by reducing inter-particle spacing in AuNP films.[39] We have evaluated these systems for methane detection and find devices using **L2a** as the ligand do not give meaningful signals even at 10% methane concentration. AuNPs capped with the 1/50 mixture of **L2b/L2a** show detectivity down to 3% methane. Overcoating polymers on devices of AuNPs capped with **L2a** provided a dramatic enhancement in sensitivity and results in clear responses to 3% methane. We thus applied such polymer overcoating to **L1d**, **L1i**, and **L1j** capped AuNPs, which were previously found to be ineffective as a result of the high device resistance. Gratifyingly, the polymer induces an apparent reduction of core-core distances and the resistance of these NP devices was lowered significantly (Table 2). These three materials in polymer overcoated devices are now capable of detecting 1000 ppm methane with 0.1-0.2% normalized resistance changes, which is a comparable performance to the other AuNPs used in this study. The responses of different AuNPs in methane detection at different lower concentrations are shown in Figure S4. Although at lower concentrations the signal-to-noise levels increased and in some cases gave erratic signals, we find that all of the phosphine capped AuNPs are capable of responding to sub-500 ppm concentrations of methane and in some cases sub-100 ppm responses are observable.

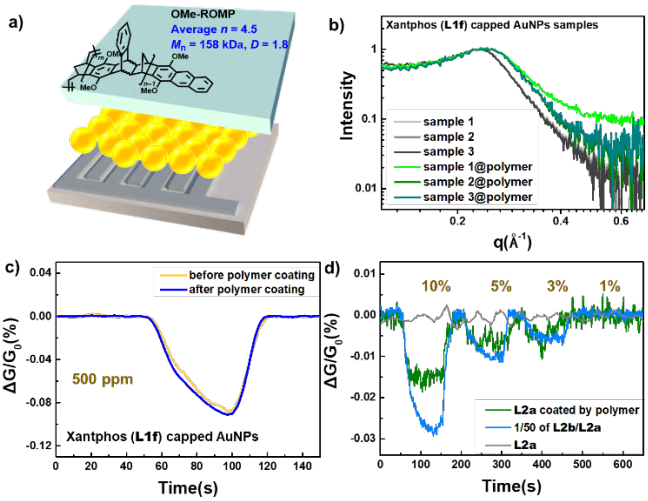

Figure 3. a) Schematic diagram of polymer overcoating of a device. b) Core-core distance was determined by SAXS (baseline subtracted). c) Sensing curve at 500 ppm of methane before and after polymer coating for Xantphos (**L1f**) capped AuNPs. d) Sensitivity in methane detection of 1-decanethiol (**L2a**), 1/50 of 1,9-nonanedithiol (**L2b**)/1-decanethiol(**L2a**) capped AuNPs and 1-decanethiol (**L2a**) capped AuNPs overcoated by polymer.

L1@polymer	Resistance (Ω)	ΔG/G₀(%) at 1000 ppm
L1d@polymer	10 M	0.11
L1i@polymer	20 M	0.20
L1j@polymer	50 M	0.10

Table 2. Resistances and sensing responses of L1d, L1i, L1j capped AuNPs at 1000 ppm of methane after polymer coating.

Among the compositions investigated, the Xantphos (**L1f**) capped AuNPs displayed the highest methane response (0.2%) to 1000 ppm and a measurable response to 100 ppm concentrations (Figure 4a). Humidity induces significant swelling and impacts the responses dramatically. Unfortunately, the impact was not mitigated by the polymer overcoating (Figure S6); however, the performance of these devices using dry air as carrier gas matched those obtained with N_2 (Figure 4b). As a result, we have selected this composition

for further optimization. In the NP production we have used stoichiometric equivalents based on the phosphine centers (0.5 equiv. of **L1f** per **L1c**) and find that increasing the amount of **L1f** to 1 equiv. or decreasing it to 0.3 equiv. both lower the sensitivity (Table S2). Hence, changes in the ligand density on the AuNPs clearly impact methane detection. The nanoparticles produced using stoichiometric amounts of **L1f** can be stored in ambient air for 3 weeks and maintain the same chemiresistive methane response (Figure 4c). Simple inspection of the sensing trace Figure S5 reveals that 60 ppm of methane is readily detectable. A linear relationship is found between the chemiresistive response and methane concentration in the range of 100-1000 ppm and from this data, the limit of detection (LoD) is calculated to be 30 ppm (Figure 4d).[40]

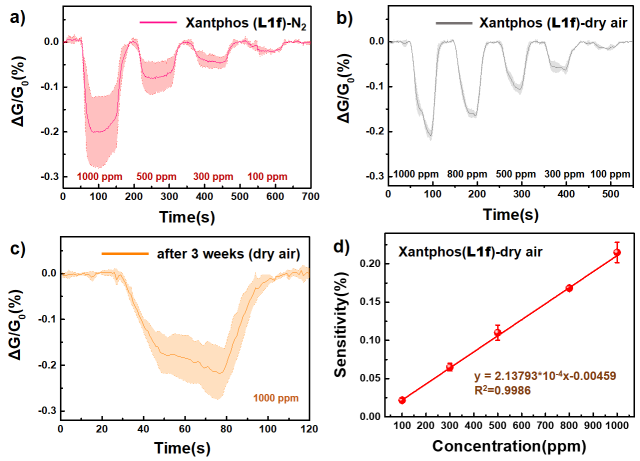

Figure 4. Methane sensing responses of Xantphos (**L1f**) capped AuNPs using a) N_2 and b) dry air as carrier gas. c) Sensitivity after 3 weeks. d) LoD of Xantphos (**L1f**) capped AuNPs. The responses and deviations are determined from 3 or more devices.

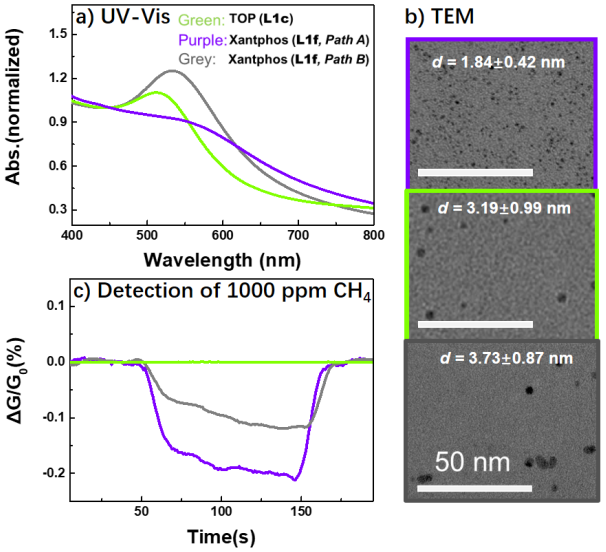

Figure 5. a) Normalized UV-Vis spectra, b) TEM images and c) sensitivity in detection of 1000 ppm methane of TOP (**L1c**) capped AuNPs (green) and Xantphos (**L1f**) capped AuNPs synthesized *via* *Path A* (purple) and *Path B* (grey).

The ability of the phosphine ligands to create voids in the AuNP films that bind methane undoubtedly contributes to their outstanding performance for methane detection. Similar concepts have been previously suggested for the aforementioned dithiol capped AuNPs. To better understand the structure property relationships at issue, we have conducted some additional experiments. To examine the role of aromatic groups, we have made use of the TOP (**L1c**) capped AuNPs, which can be evaluated using an N_2 carrier gas. We find that with freshly prepared AuNPs having these alkyl phosphine capping ligands, there is no response to 1000 ppm of methane (Figure 5c, green). Hence, simple partitioning of methane into alkane coatings surrounding the AuNPs is not adequate to produce a sensing response. Computational results show that free PPh_3 and CH_4 have a 2.70 kcal/mol binding energy in the gas phase, which suggests that the expected CH-π interactions assist in promoting methane binding and sensing responses (see Supporting Information for the computational details). The size of the AuNPs is critical to their performance and using the two-step ligand exchange method, we were able to obtain Xantphos (**L1f**) capped AuNPs with $d = 3.73 \pm 0.87$ nm *via* *Path B* (Figure 5b, grey) that are twice as large as the ones synthesized directly *via* *Path A* ($d = 1.84 \pm 0.42$ nm, Figure 5b, purple). The size difference of these NPs is apparent by analysis of the UV-Vis spectra (Figure 5a). The flatter curve (*Path A*) fits well with the AuNPs larger than 1 nm but smaller than 2.5 nm,[32] whereas the UV-Vis bands for those obtained by *Path B* are representative of materials with diameters of 3–5 nm.[35] As mentioned earlier, the exchange of **L1c** with chelating phosphines promotes Ostwald ripening of the AuNPs. This latter effect is also revealed in UV-Vis spectra where the produced **L1f** capped AuNPs (*Path B*) have a red-shifted absorption maximum at 533 nm as compared with their precursor **L1c** capped AuNPs (*ca.* 518 nm). These **L1f** capped AuNPs show an inverse correlation of sensitivity with size, with the smaller particles produced by *Path A* displaying a 0.2 % response and the larger particles made by ligand exchange (*Path B*) having a 0.1% response to a 1000 ppm methane (Figure 5c). To further confirm the impact of AuNP size, we later prepared dppe (**L1d**) capped AuNPs at different size and the same trend was revealed (Figure S9). The fact that smaller core size increases the sensitivity is potentially the result of higher surface area-to-volume ratio, as well as methane binding sites obtained by packing of the phosphine ligands around smaller AuNPs.

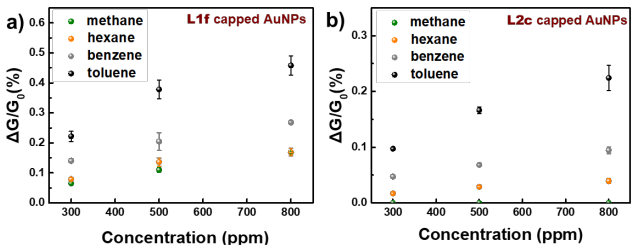

Figure 6. a) Xantphos (**L1f**) and b) 4-toluenethiol (**L2c**) capped AuNPs to selected hydrocarbons at 300, 500 and 800 ppm. The error bars are determined from 3 or more devices.

In any sensor system, selectivity within a range of analytes that may be encountered is always important, and hence we have conducted a study of the response of **L1f** capped AuNPs (*Path A*) to a panel of hydrocarbons. The response of this system to 500 ppm toluene ($\Delta G/G_0 = 0.38\%$) is higher than that for 500 ppm benzene ($\Delta G/G_0 = 0.21\%$), which is consistent with the expected portioning of the higher boiling point solvent into the sensor film (Figure 6a). Perhaps more interesting is the

observation that the response to 500 ppm hexane ($\Delta G/G_0$ = 0.14%) is nearly the same as to methane ($\Delta G/G_0$ = 0.11%) at the same concentration. A sensor array of different capped AuNPs can be potentially constructed to differentiate methane from other hydrocarbons. We were particularly interested to see if we can use the differences between thiol- and phosphine-based caps to produce differential responses. To this end, we utilized 4-toluenethiol (**L2c**) capped AuNPs, which has been previously studied in hydrocarbon sensing,[36] and have contrasted them to **L1f** capped AuNPs. The **L2c** system has a slightly lower sensitivity to hexane ($\Delta G/G_0$ = 0.03%), benzene ($\Delta G/G_0$ = 0.05%), and toluene ($\Delta G/G_0$ = 0.17%) at 500 ppm (Figure 6b). However, although it does respond to high concentrations of methane, it has no measurable response to *ca.*3 % methane, a concentration that is near the explosion limit (Figure S8). To contrast these materials, the responses of **L1f** and **L2c** capped AuNPs to hexane, benzene, toluene, and methane at 300, 500, and 800 ppm are respectively shown in Figure 6a and 6b. Although, the responses to hexane, benzene and toluene are roughly comparable between the systems, the **L2c** capped AuNPs lacks a methane response. As a result, with just two sensors, it is possible to differentiate methane from these other hydrocarbons. The contrast between the selected pair is not unique, and we have also examined AuNPs capped with a long-chain alkyl thiol, a dithiol, and an aromatic thiol for methane detection. They all displayed comparable gold/ligand ratios and exhibits intact shells on the gold surface (see supporting information for details), but none of them are capable of detecting methane under *ca.* 3%.

CONCLUSION

In the course of studies in methane detection based on phosphine capped AuNPs, we developed two mild synthetic routes to phosphine capped AuNPs with different diameters, which is the key in generating intact ligand shells. Thus, methane detection at ppm level was realized in AuNP-based sensing platform. Polymer-overcoating produced effects similar to that of dithiols by reducing the core-core distances between AuNPs, and provide more optimal conductivities for sensing. We demonstrated that various commercially available aromatic phosphine ligands are capable of providing functional caps on AuNPs that enable the detection of ppm concentrations of methane. Phosphine capped AuNPs nicely complement conventional thiol capped AuNPs in VOC detention. These studies provide important insights that will direct future phosphine-capped AuNP-based applications.

METHODS

Materials: The following chemicals were used as received: phosphine ligands (**L1b**-**L1k**, purchased from Sigma-Aldrich or Alfa Aesar), thiol ligands (**L2a**-**L2c**, purchased from Sigma-Aldrich), triphenylphosphine gold(I) chloride (purchased from Alfa Aesar), gold(III) chloride hydrate ($HAuCl_4$, > 99.9 %, purchased from Nanopartz), tetraoctylammonium bromide (purchased from Sigma-Aldrich), tertbutylamine-borane (purchased from Sigma-Aldrich). A gas cylinder containing methane (100 %, ultrahigh purity) was purchased from Airgas. Interdigitated electrodes (DRP-G-IDEPT5) were purchased from Metrohm DropSens.

*Synthesis of AuCl(**L1**).* General Procedure: 1) To a methanol solution (5 mL) of $HAuCl_4 \cdot 3H_2O$ (200 mg, 0.48 mmol) was added Me_2S (0.3 mL), and the mixture was stirred at room temperature for 1 hour. The reaction mixture was filtrated and washed by MeOH. White solids were obtained in 95% yield (134 mg). 2) To a CH_2Cl_2 solution (3 mL) of 0.1 mmol $Au(SMe_2)Cl$, 0.1 mmol of mono-phosphine or 0.05 mmol of chelating phosphine ligands were added and the mixture was stirred at room temperature for 1 hour. The solvent was removed by evacuation for further synthesis.

*Preparation of **L1a-L1j** capped AuNPs (Path A)*: 0.1 mmol of AuCl(**L1**) and 0.088g of tertbutylamine-borane powder were mixed in 16 mL of benzene to form a clear solution. The mixture was kept stirring at 80 ºC for 3 hours and centrifuged at 10000 rpm for 10 min. To further purification, the mixtures were centrifuged at 12633g for another 10 min in toluene.

*Preparation of **L1d**, **L1e**, **L1k** capped AuNPs via ligand exchange (Path B)*: 0.1 mmol of AuCl(TOP) and 0.088g of tertbutylamine-borane powder were mixed in 16 mL of benzene to form a clear solution. The mixture was kept stirring at 80 ºC for 3 hours and cooled down to room temperature. 1 equiv. the ligand was added into the reaction vial. Mixtures were heated to 50 ºC, reacted for another 4 hours and centrifuged at 10000 rpm for 10 min. To further purification, the mixtures were centrifuged at 12633g for another 10 min in toluene.

*Preparation of **L2a-L2c** capped AuNPs (typical Brust Procedure)*: an aqueous solution of $HAuCl_4 \cdot 3H_2O$ (0.0402 g, 0.102 mmol) in deionized water (3.2 mL) was mixed with a solution of tetraoctylammonium bromide (TOAB) (0.228 g, 4.17 mmol) in toluene (8 mL). The two-phase mixture was vigorously stirred until all the tetrachloroaurate was transferred into the organic layer, and a solution of thiol (2 equiv., 0.204 mmol) in toluene (1 mL) was then added. The mixture was stirred for 20 min. A freshly prepared aqueous solution of sodium borohydride (0.0393 g, 1.1 mmol) in deionized water (5 mL) was rapidly added with vigorous stirring. After further stirring for 3 h, the organic phase was separated, washed with DI water, and then reduced to 1 mL in a rotary evaporator. After the addition of 20 mL of ethanol, the mixture was kept overnight at -18 °C and then centrifuged at 12633g for 10 min.

Characterization: To characterize AuNPs and ligand shells, and transmission electron microscope (TEM, FEI-Tecnai) and X-ray photoelectron spectroscopy (XPS, thermo scientific KAlpha+) were used. NMR was performed on a Bruker Avance III DRX 400 MHz instrument. X-ray diffraction (XRD) was performed with a SAXSLAB instrument equipped with a Rigaku 002 microfocus X-ray source (CuKα = 1.5409 Å) and a Dectris Pilatus 300K detector that moves from 100 mm to 1500 mm from the sample. The beam center and the q range were calibrated using the diffraction peaks of silver behenate.

General Procedure for Methane Sensing Measurements: 8 µL of gold nanoparticle suspension in toluene was drop-casted on platinum electrodes and the device was enclosed in a homemade Teflon gas flow chamber. The carrier gas was held constant at 10 L/min. The resistance of the device was measured over time (1 scan/sec), with typical parameters including 10 min equilibration time (for the baseline resistance to stabilize) followed by 50 s exposure to methane and then 50 s of recovery.

ASSOCIATED CONTENT

Supporting Information. The Supporting Information is available free of charge on the ACS Publications website.

Characterization of AuNPs (TEM, XPS, XRD); Additional Methane Detection Data (Low Concentrations, Optimization, Humidity Study, Control Experiments); Computational Studies (PDF).

The authors declare no competing financial interest.

AUTHOR INFORMATION

Corresponding Author

tswager@mit.edu

ACKNOWLEDGMENT

This research was supported by Eni S.p.A. through the MIT energy initiative and the National Science Foundation (DMR 1809740).

REFERENCES

(1) Dykmana, L.; Khlebtsov, N. Gold Nanoparticles in Biomedical Applications: Recent Advances and Perspectives. *Chem. Soc. Rev.* **2012**, *41*, 2256–2282.

(2) Dreaden, E.; Alkilany, A.; Huang, X.; Murphy, C.; El-Sayed, M. The Golden Age: Gold Nanoparticles for Biomedicine. *Chem. Soc. Rev.* **2012**, *41*, 2740–2779.

(3) Zhou, W.; Gao, X.; Liu, D.; Chen, X. Gold Nanoparticles for *In Vitro* Diagnostics. *Chem. Rev.* **2015**, *115*, 19, 10575−10636.

(4) Grzelczak, M.; Liz-Marzán, L.; Klajn, R. Stimuli-Responsive Self-Assembly of Nanoparticles. *Chem. Soc. Rev.* **2019**, *48*, 1342−1361.

(5) Saha, K.; Agasti, S.; Kim, C.; Li, X.; Rotello, V. Gold Nanoparticles in Chemical and Biological Sensing. *Chem. Rev.* **2012**, *112*, 2739−2779.

(6) San, K.; Shon, Y. Synthesis of Alkanethiolate-Capped Metal Nanoparticles Using Alkyl Thiosulfate Ligand Precursors: A Method to Generate Promising Reagents for Selective Catalysis. *Nanomaterials* **2018**, *8,* 346−366.

(7) Xie, Z.; Raju, M.; Stewart, A,; Nantz, M.; Fu, X. Imparting Sensitivity and Selectivity to a Gold Nanoparticle Chemiresistor through Thiol Monolayer Functionalization for Sensing Acetone. *RSC Adv*. **2018**, *8*, 35618−35624.

(8) Crudden, C.; Horton, H.; Narouz1, M.; Li, Z.; Smith, C.; Munro, K.; Baddeley, C.; Larrea, C.; Drevniok, B.; Thanabalasingam, B.; McLean, A.; Zenkina, O.; Ebralidze, I.; She, Z.; Kraatz, H.; Mosey, N.; Saunders, L.; Yagi, A. Simple Direct Formation of Self-Assembled N-Heterocyclic Carbene Monolayers on Gold and Their Application in Biosensing. *Nat. Commun*. **2016**, *7*, 1-7.

(9) Man, R.; Li, C.; MacLean, M.; Zenkina, O.; Zamora, M.; Saunders, L.; Rousina-Webb, A.; Nambo, M.; Crudden, C. Ultrastable Gold Nanoparticles Modified by Bidentate N-Heterocyclic Carbene Ligands. *J. Am. Chem. Soc.* **2018**, *140*, 1576−1579.

(10) MacLeod, M.; Goodman, A.; Ye, H.; Nguyen, H.; Voorhis, T.; Johnson, J. Robust Gold Nanorods Stabilized by Bidentate N-Heterocyclic-Carbene-Thiolate Ligands. *Nat. Chem.* **2019**, *11*, 57–63.

(11) Schmid, G.; Pfeil, R.; Boese, R.; Bandermann, F.; Meyer, S.; Calis, G. H. M.; van der Velden, J. W. A. $Au_{55}[P(C_6H_5)_3]_{12}Cl_6$-ein Gold Cluster ungewöhnlicher Größe. *Chem. Ber.* **1981**, *114*, 3634−3642.

(12) Weare, W.; Reed, S.; Warner, M.; Hutchison, J. Improved Synthesis of Small (d_{CORE}~1.5 nm) Phosphine-Stabilized Gold Nanoparticles. *J. Am. Chem. Soc.* **2000**, *122*, 12890−12891.

(13) Tamura, M.; Fujihara, H. Chiral Bisphosphine BINAP-Stabilized Gold and Palladium Nanoparticles with Small Size and Their Palladium Nanoparticle-Catalyzed Asymmetric Reaction. *J. Am. Chem. Soc*. **2003**, *125*, 15742−15743.

(14) Moores, A.; Goettmann, F.; Sanchez, C.; Floch, P. Phosphine Stabilised Gold Nanoparticles; Synthesis and Immobilization on Mesoporous Materials. *Chem. Commun.* **2004**, 2842−2843.

(15) Yanagimoto, Y.; Negishi, Y.; Fujihara, H.; Tsukuda, T. Chiroptical Activity of BINAP-Stabilized Undecagold Clusters. *J. Phys. Chem. B.* **2006**, *110*, 11611–11614.

(16) Shem, P.; Sardar, R.; Shumaker-Parry, J. One-Step Synthesis of Phosphine-Stabilized Gold Nanoparticles Using the Mild Reducing Agent 9-BBN. *Langmuir* **2009**, *25*, 13279–13283.

(17) Silva, N.; Ha, J-M.; Solovyov, A.; Nigra, M. M.; Ogino, I.; Yeh, S.; Durkin, K. A.; Katz, A. A Bioinspired Approach for Controlling Accessibility in Calix[4]arene-Bound Metal Cluster Catalysts. *Nat. Chem*. **2010**, *2*, 1062–1068.

(18) Cano, I.; Huertos, M. A.; Chapman, A. M.; Buntkowsky, G.; Gutmann, T.; Groszewicz, P. B.; Leeuwen, P. Air-Stable Gold Nanoparticles Ligated by Secondary Phosphine Oxides as Catalyst for the Chemoselective Hydrogenation of Substituted Aldehydes: A Remarkable Ligand Effect. *J. Am. Chem. Soc.* **2015**, *137*, 7718−7727.

(19) Woehrle, G.; Brown, L.; Hutchison, J. Thiol-Functionalized, 1.5-nm Gold Nanoparticles through Ligand Exchange Reactions: Scope and Mechanism of Ligand Exchange. *J. Am. Chem. Soc.* **2005**, *127*, 2172–2183.

(20) Goubet, N.; Portalès, H.; Yan, C.; Arfaoui, I.; Albouy, P.; Mermet, A.; Pileni, M. Simultaneous Growths of Gold Colloidal Crystals. *J. Am. Chem. Soc.* **2012**, *134*, 3714−3719.

(21) Wang, W.; Murray, R. Reaction of Triphenylphosphine with Phenylethanethiolate-Protected Au38 Nanoparticles. *Langmuir* **2005**, *21*, 7015–7022.

(22) Sun, Q.; Aguila, B.; Verma, G.; Liu, X.; Dai, Z.; Deng, F.; Meng, X. Xiao, F.; Ma, S. Superhydrophobicity: Constructing Homogeneous Catalysts into Superhydrophobic Porous Frameworks to Protect Them from Hydrolytic Degradation. *Chem* **2016**, *1*, 628–639.

(23) Cai, R.; Ye, X.; Sun, Q.; He, Q.; He, Y.; Ma, S.; Shi, X. Anchoring Triazole-Gold(I) Complex into Porous Organic Polymer to Boost the Stability and Reactivity of Gold(I) Catalyst. *ACS Catal*. **2017**, *7*, 1087−1092.

(24) Schiermeier, Q.; Methane Finding Baffles Scientists, *Nature* **2006**, *439*, 128–128 (News).

(25) Roshan, H.; Mosahebfard, A.; Sheikhi, M. H. Effect of Gold Nanoparticles Incorporation on Electrical Conductivity and Methane Gas Sensing Characteristics of Lead Sulfide Colloidal Nanocrystals. *IEEE Sens. J*. **2018**, *18*, 1940–1945.

(26) Bhattacharyya, P.; Basu, P.K.; Saha, H.; Basu, S. Fast Response Methane Sensor Using Nanocrystalline Zinc Oxide Thin Films Derived by Sol-Gel Method. *Sensors and Actuators B* **2007**, *124*, 62–67.

(27) Comert, B.; Akin, N.; Donmez, M.; Saglam, S.; Ozcelik, S. Titanium Dioxide Thin Films as Methane Gas Sensors. *IEEE Sens. J*. **2016**, *16*, 8890–8896.

(28) Khoshaman, A.; Li, P.; Merbouh, N.; Bahreyni, B. Highly Sensitive Supra-Molecular Thin Films for Gravimetric Detection of Methane. *Sensors and Actuators B: Chemical* **2012**, *161*, 954–960.

(29) Zheng, N.; Fan, J.; Stucky, G. One-Step One-Phase Synthesis of Monodisperse Noble-Metallic Nanoparticles and Their Colloidal Crystals. *J. Am. Chem. Soc.* **2006**, *128*, 6550–6551.

(30) Mézailles, N.; Ricard, L.; Gagosz, F. Phosphine Gold(I) Bis-(trifluoromethanesulfonyl)imidate Complexes as New Highly Efficient and Air-Stable Catalysts for the Cycloisomerization of Enynes. *Org. Lett.* **2005**, *7*, 19, 4133–4136.

(31) Son, S.; Jang, Y.; Yoon, K.; Kang, E.; Hyeon, T. Facile Synthesis of Various Phosphine-Stabilized Monodisperse Palladium Nanoparticles through the Understanding of Coordination Chemistry of the Nanoparticles. *Nano Lett.* **2004**, *4*,1147–1151.

(32) Pettibone, J.; Hudgens, J. Gold Cluster Formation with Phosphine Ligands: Etching as a Size-Selective Synthetic Pathway for Small Clusters? *ACS Nano*. **2011**, *5*, 2989–3002.

(33) Moores, A.; Goettmann, F.; Sanchez, C.; Floch, P. Phosphinine Stabilised Gold Nanoparticles; Synthesis and Immobilization on Mesoporous Materials. *Chem. Commun.* **2004**, *24*, 2842–2843.

(34) Ha, J-M.; Solovyov, A.; Katz, A. Synthesis and Characterization of Accessible Metal Surfaces in Calixarene-Bound Gold Nanoparticles. *Langmuir* **2009**, *25*, 10548–10553.

(35) Nealon, G.; Donnio, Bertrand.; Greget, R.; Kappler, J.; Terazzib, E.; Gallani, J. Magnetism in Gold Nanoparticles. *Nanoscale* **2012**, *4*, 5244–5258.

(36) Evans, S.; Johnson, S.; Cheng, Y.; Shen, T. Vapour Sensing Using Hybrid Organic-Inorganic Nanostructured Materials. *J. Mater. Chem*. **2000**, *10*, 183–188.

(37) Zhao, Y.; He, Y.; Swager, T. Porous Organic Polymers *via* Ring Opening Metathesis Polymerization. *ACS Macro Lett.* **2018**, *7*, 300–304.

(38) Wohltjen, H.; Snow, A. Colloidal Metal-Insulator-Metal Ensemble Chemiresistor Sensor. *Anal. Chem.* **1998**, *70*, 2856–2859.

(39) Wang, W.; Shi, X.; Kariuki, N.; Schadt, M.; Wang, G.; Deng, Q.; Choi, J.; Luo, J.; Lu, S.; Zhong, C. Array of Molecularly Mediated Thin

Film Assemblies of Nanoparticles: Correlation of Vapor Sensing with Interparticle Spatial Properties. *J. Am. Chem. Soc*. **2007**, *129*, 7, 2161–2170.

(40) Mirica, K. A.; Weis, J. G.; Schnorr, J. M.; Esser, B.; Swager, T. M. Mechanical Drawing of Gas Sensors on Paper. *Angew. Chem. Int. Ed.* **2012**, *51*, 10740–10745.

Graphic Abstract